INTERNATIONAL JOURNAL OF Electroactive Materials

Int. J. Electroactive Mater. **5 (2017) 42-49**
www.electroactmater.com

RECEIVED
31 May 2017

REVISED
14 June 2017

ACCEPTED FOR PUBLICATION
16 June 2017

PUBLISHED
27 November 2017

Solid-State Hybrid Supercapacitor of PEDOT:PSS//$LiFePO_4$ Configuration Fabricated with Gel Polymer Electrolyte

Manoj K. Singh[a*], S.A. Hashmi[b]

[a]Department of Physics, Swami Shraddhanand College, University of Delhi, Delhi-110036, India
[b]Department of Physics & Astrophysics, University of Delhi, Delhi-110007, India
E-mails: mmanoj.ssi@gmail.com*, sahashmi@physics.du.ac.in*

ABSTRACT: Hybrid BatCap, a latest generation of hybrid supercapacitor, has the possibility to overcome the energy density limitation of the symmetric supercapacitor configuration and the power density limitation in lithium-ion batteries. We report the comparative performance of symmetric pseudocapacitor PEDOT:PSS//PEDOT:PSS and hybrid BatCap PEDOT:PSS//$LiFePO_4$ employed with polymer electrolyte (GPE) as electrolyte/separator. A free-standing, flexible film comprising of 1M lithium bis(trifluoromethanesulfonyl)imide (LiTFSI) in ionic liquid 1-butyl-1-methyl pyrrolidinium bis(trifluoromethanesulfonyl)imide (BMPTFSI) immobilized in poly(vinylidene fluoride-co-hexafluoro-propylene) (PVdF-HFP) shows excellent properties such as electrochemical window of 2.9 V and high ionic conductivity of 1.38×10^{-3} S cm^{-1} at room temperature. The performance characteristics of supercapacitor have been evaluated by electrochemical impedance spectroscopy (EIS), cyclic voltammetry (CV) and galvanostatic charge/discharge techniques. The hybrid BatCap PEDOT:PSS//$LiFePO_4$ has been found to offered better performance in terms of specific capacity (29.4 mA h g^{-1}), specific energy (21.3 Wh kg^{-1}) and specific power (1.2 kW kg^{-1}) as compared to symmetric pseudocapacitor PEDOT:PSS//PEDOT:PSS.
Keywords: Hybrid BatCaps, Gel polymer electrolyte, Lithium iron phosphate, Conducting polymer.

1. Introduction

The development of new energy sources and improvement in energy efficiency in existing storage devices are the major concerns of the current global research. Broadly, devices for electrochemical energy storage include rechargeable batteries and supercapacitors [1, 2]. The supercapacitors attract global research interest due to high capacitance values with large cycle life and high power density [1-3]. Such features make them superior over the other energy storage devices for their practical exploitations. The supercapacitors are useful for a wide range of applications for power backup in renewable energy sources and portable electronics, medical utilities and military appliances and hybrid electric vehicles (HEVs) [4].

Basically, two types of mechanisms are involved to store the charges in supercapacitors namely, electric double layer (electrostatic) and pseudocapacitor (fast-faradaic) [1, 2, 5]. In general, high surface area carbons (activated carbon, MWCNTs, GO, rGO, etc.) are being used as electrode materials in electric double layer capacitors (EDLCs), whereas noble metal oxides (e.g. RuO_2, MnO_2, NiO etc.) or conducting polymers (like polyaniline, polypyrrole, etc.) are used in pseudocapacitors. From the configuration point of view, the performance of symmetric supercapacitors is limited especially energy density due to limited voltage range [6]. To enhance the performance of supercapacitors, hybrid configuration comes into focus in which both types of charge storage mechanisms occur in a single device. Hybrid supercapacitor, the latest generation configuration of supercapacitor, has the possibility to overcome the energy density limitation of existing supercapacitors and the power density limitation in lithium-ion batteries [7]. Hybrid battery-capacitor (BatCap) is one of the classes of hybrid supercapacitor which employ the combination of a capacitor electrode and a battery electrode. The capacitor electrode provides high power density whereas a battery electrode ensures the high specific energy [8, 9].

Among different conducting polymers, poly(3,4-ethylenedioxythiophene) (PEDOT) is promising one as supercapacitor electrodes because of the unprecedented stability and faster redox transitions [10]. Further, the olivine $LiFePO_4$ cathode material has become recently popular cathode materials in lithium-ion battery due to its low cost, environment-friendly nature, high specific capacity (~170 mA h g^{-1}) and good cyclic efficiency (>2000 cycles) etc. [11, 12]. In the present work, a hybrid BatCap system has been proposed using PEDOT:PSS and $LiFePO_4$ electrodes to enhance the performance of supercapacitor.

Supercapacitors, reported in the literature, are generally employed with liquid electrolytes [13], which suffer from various drawbacks like leakage, corrosion, bulky design and self-discharge etc. Gel polymer electrolytes (GPEs) are found to be excellent substitute of liquid electrolytes for their applications in supercapacitors due to their many advantages, particularly, for the miniaturization, safety, and dimensional stability [14]. GPEs are generally prepared by immobilizing the liquid electrolyte (e.g. $LiCF_3SO_3$ in propylene carbonate) in the host polymers such as PVdF-HFP, PMMA, etc. [14, 15]. They offer a highly

conducting liquid like transport of ions and solid state like mechanical properties. Recently, room temperature ionic liquids (RTILs), which are thermally stable and high ionic conductivity molten salts, are used as solvents/plasticizers in GPEs [16].

In this study, the $LiFePO_4$ cathode has been synthesized and characterized. A GPE film composed of LiTFSI/BMPTFSI liquid electrolyte entrapped in PVdF-HFP, has been used as electrolyte/separator to fabricate solid-state supercapacitors. The comparative performance studies are presented on solid-state symmetrical pseudocapacitor using PEDOT:PSS and hybrid BatCap employing $LiFePO_4$ cathode and PEDOT:PSS capacitive electrode. The performance of supercapacitor cells has been analyzed using the electrochemical impedance spectroscopy (EIS), cyclic voltammetry (CV) and galvanostatic charge/discharge techniques.

2. Experimental

2.1 Materials

The copolymer, PVdF-HFP (M.W.~4×10^5), ionic liquid 1-butyl-1-methyl pyrrolidinium bis (trifluoromethylsulfonyl) imide (BMPTFSI), and salt lithium bis (trifluoromethanesulfonyl) imide (LiTFSI) were procured from Sigma-Aldrich and vacuum-dried overnight at 80 ^oC. The precursor materials, namely, lithium acetate dihydrate ($CH_3COOLi.2H_2O$, M.W.=102.02, 98%), ferrous oxalate dihydrate ($FeC_2O_4.2H_2O$, M.W.=179.89, 99%), ammonium dihydrogen phosphate ($NH_4H_2PO_4$, M.W.=1.1503,99.9 %) and PEDOT:PSS solution (1.3 wt.% in water) were also procured from Sigma-Aldrich and used without further purification.

2.2 Preparation and Characterization of Gel Polymer Electrolyte

The gel electrolyte was prepared by "solution-cast method", in which liquid electrolyte 1M LiTFSI in ionic liquid (BMPTFSI) was immobilized in the solution of PVdF-HFP in acetone maintaining liquid electrolyte and polymer ratio of 80:20 (wt/wt). This solution was stirred magnetically at room temperature for 24 hours and cast over the glass petri-dishes. After the complete evaporation of acetone, semitransparent, flexible GPE films were obtained and stored in dry box for further characterizations. The electrochemical performance of the GPE films was tested by measuring ionic conductivity and electrochemical stability window (ESW) using Broadband Dielectric/Impedance Analyzer (C-50 Alpha A, Novocontrole, Germany) and an electrochemical workstation (660E, CH Instruments, USA), respectively.

2.3 Preparation and Characterization of Electrodes

The cathode material $LiFePO_4$ was synthesized using a "sol-gel" precursor method, as described by us earlier [17]. In the process, lithium acetate dihydrate ($CH_3COOLi{\cdot}2H_2O$), ferrous oxalate dihydrate ($FeC_2O_4{\cdot}2H_2O$) and ammonium dihydrogen phosphate ($NH_4H_2PO_4$) were dissolved in a minimum amount of ethylene glycol in equal stoichiometric ratio followed by heating at 800 °C for 15 hours in N_2 atmosphere. After cooling the material slowly to room temperature, a blackish $LiFePO_4$ powder was obtained. The synthesized $LiFePO_4$ was chactererized by XRD (D8-Discover, Bruker, USA), surface area and pore size analyzer (Gemini-V, Micromeritics, USA) and SEM (Mira-3, TESCAN) recorded in low vacuum after sputtering gold on the sample.

For the preparation of cathode of hybrid BatCap, a slurry was prepared by mixing graphite powder (10%), binder (PVdF-HFP, 20%) in $LiFePO_4$. The slurry was spin-coated on flexible graphite sheet (250 µm thick, Nickunj Eximp Entp., India) and dried at 90 ºC overnight. The negative electrode was prepared by drop-cast of diluted PEDOT:PSS solution on graphite sheet followed by heating 100 ºC overnight. The mass of $LiFePO_4$ and PEDOT:PSS active electrode materials were 0.62 mg cm^{-2}.

2.4 Fabrication and Characterization of Supercapacitors

The supercapacitors were fabricated by the following procedures. The dilute slurry of GPE was coated on both electrodes separately and dried. Two such systems were stacked over each other such that the GPE is sandwiched between two electrodes to obtain full cell. The two cells have been prepared with the following configurations:

Cell#1: PEDOT:PSS | GPE | PEDOT:PSS (Pseudocapacitor)

Cell#2: PEDOT:PSS | GPE | $LiFePO_4$ (Hybrid BatCap)

The comparative performance of the cells was measured on the same electrochemical analyzer mentioned above. The EIS of the supercapacitor cells was carried out in the frequency range from 10 mHz to 100 kHz with amplitude voltage of 0.01 V. The CV was performed at different scan rates in different floating potentials. The galvanostatic charge–discharge text was performed at constant current density at 1 mA cm^{-2}.

3. Results and discussion

3.1 Electrochemical Characterization of GPE

Fig. 1(a) depicts the Bode plot (σ vs. frequency) of the GPE PVdF-HFP/BMPTFSI/LiTFSI which was recorded at room temperature (27 ^{o}C). The conductivity was evaluated on the cell: SS | GPE film | SS, where SS stands for stainless steel working as a blocking/irreversible electrode. The GPE film offers the conductivity of 1.38×10^{-3} S cm^{-1} (evaluated from plateau region of the Bode plot), which is slightly lower than PVdF-HFP/BMPTFSI (1.52×10^{-3} S cm^{-1}) [18]. This is due to the possible increase in viscosity of the ionic liquid, when Li-salt was added in ionic liquid. However, this order of conductivity is close to that of liquid electrolytes. The electrochemical stability window (ESW) of the GPE has been examined by LSV technique recorded at a scan of 5 mV s^{-1} using the cell: SS | GPE film | Ag, where SS as a working electrode and Ag as both the counter and the reference electrodes. This ESW is found to be 2.9 V, which shows the anodic limit of the electrolyte, which is ascribed to the reduction of cations (Li^+ and BMI^+ as in the present case) [19]. The high conductivity and sufficient electrostablity window of GPE shows its applicability in supercapacitors application as electrolyte/separator.

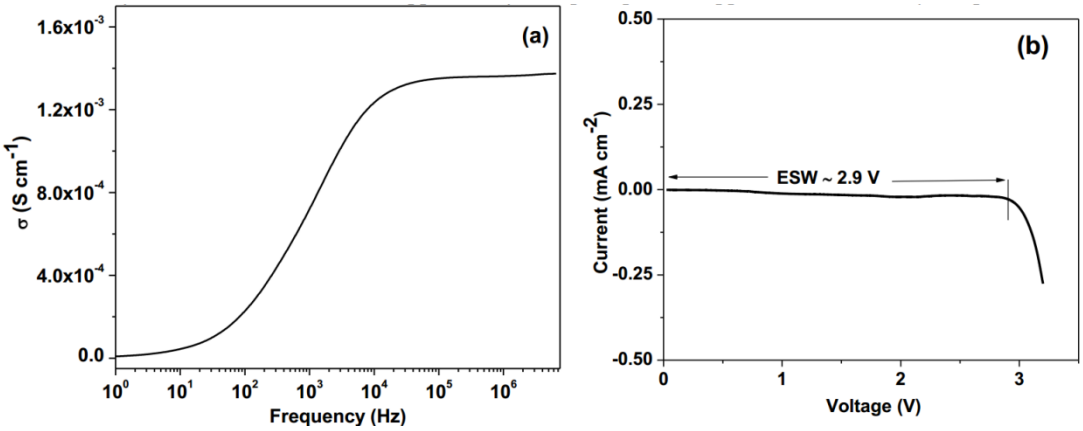

Figure 1: (a) Bode plot and (b) LSV response of GPE film at room temperature (27 °C).

3.2 Characterization of $LiFePO_4$ cathode

The XRD pattern of pristine $LiFePO_4$ is depicted in **Fig. 2(a)**. The XRD peaks of the as-synthesized pristine $LiFePO_4$ are well indexed as per the JCPDS No. 00-040-1499, indicating the absence of any impurity. The observed XRD peaks indicate the orthorhombic olivine structure of $LiFePO_4$ having space group Pmnb with lattice parameters, a = 6.0189 Å, b = 10.3470 Å and c = 4.7039 Å [20]. The N_2 adsorption–desorption isotherms of the pristine $LiFePO_4$ shown in Fig. 2(b). The BET surface area of $LiFePO_4$ has been found to be 20 m^2 g^{-1}. According to the IUPAC classification, the $LiFePO_4$ powder shows the type-*IV* isotherm [21], in which a very small jump indicates micro-porosity followed by a gradual increase showing mesoporosity in the isotherms with respect to the relative pressure. The hysteresis loop during N_2 desorption has also been observed, which also indicates mesoporous interiors in the pristine $LiFePO_4$ [22]. The morphology of $LiFePO_4$ particles (obtained from by sol-gel method) is observed to be micro-spherical with non-uniform particle sizes as shown in the SEM image (**Fig. 2(b)** inset).

3.3 Performance studies of supercapacitors

Fig. 3 shows the comparative EIS plots of symmetric pseudocapacitor (cell 1) and hybrid BatCap (cell 2). The expanded representation of the EIS plots in the high frequency region is also shown in the respective insets of **Fig. 3**. It is observed that the *Z*" versus *Z*' plot rises steeply for the cell 1 in the lower frequency range. This indicates the capacitive nature of the interfaces formed by pure PEDOT-PSS with Li-ion conducting GPE (PVdF-HFP/BMPTFSI/LiTFSI). The EIS plot of hybrid BatCap cell 2 is completely different from symmetric pseudocapacitor cell 1. It is composed of almost by a slash with 45º in the middle and lower frequency region due to the resistive $LiFePO_4$ electrode as shown in **Fig. 3(b)**. The value of bulk resistance, R_b is also referred as equivalent series resistance (ESR) of the cell could be evaluated from the intercepts on the real axis of the EIS plot. The overall resistance, R* of the cell is also estimated at 10 mHz.

These parameters, including overall capacitance (C_o) of the cell and specific capacitance (C_{sp}) of electrode (PEDOT:PSS) have been evaluated and listed in **Table 1**.

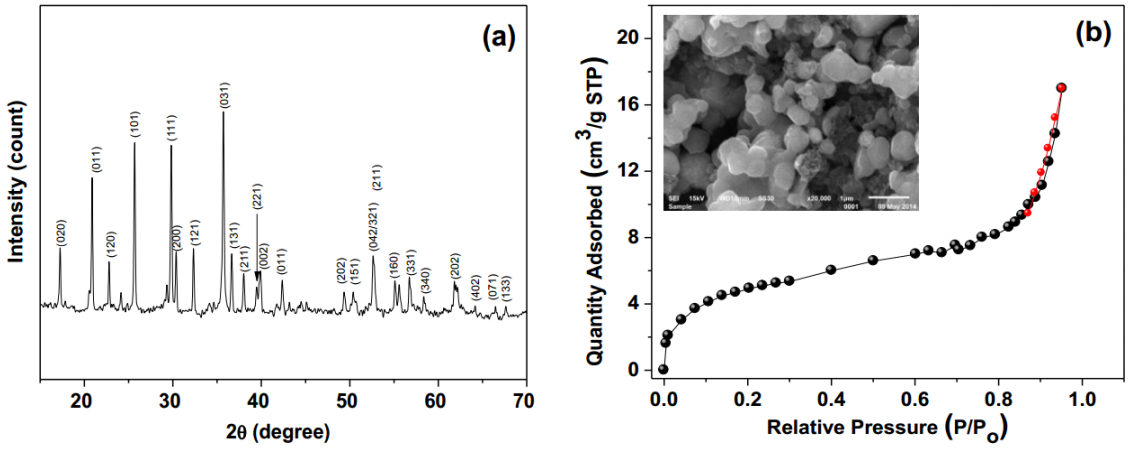

Figure 2: (a) XRD pattern and (b) N_2-adsorption-desorption isotherms of the pristine $LiFePO_4$. SEM image is shown as inset.

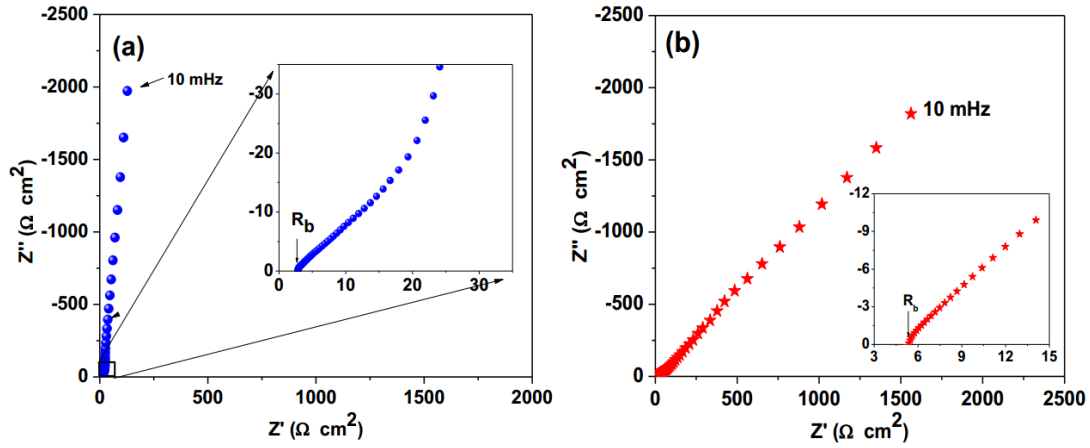

Figure 3: Electrochemical impedance spectra of (a) pseudocapacitor cell and (b) hybrid BatCap cell.

The overall capacitance (C_o) of the cells can be estimated from the expression [23, 24],

$$\frac{1}{C_o} = \frac{1}{C_1} + \frac{1}{C_2} \tag{1}$$

C_1 and C_2 are single electrode capacitances of individual interfaces. For the symmetric supercapacitor, the capacitance of C_1 and C_2 are almost equal. Hence, the single electrode specific capacitance can be evaluated by $C_{sp} = C_1/m = 2C_o/m$. While, in the case of hybrid BatCap (the combination of capacitor and battery interfaces), the battery interface (say C_2) is infinite capacitance [23, 25] and full charges are stored on C_1 at the capacitor interface. Thus, the specific capacitance of capacitive electrode of the hybrid BatCap cell 2 has been evaluated from the expression: $C_{sp} = C_1/m = C_o/m$, where $C_o = -1/(2\pi fZ'')$, where Z'' is the imaginary impedance at applied low frequency (10 mHz in the present case) and m is the mass of single PEDOT:PSS capacitive electrode. The capacitance performance of PEDOT:PSS (observed in cell 2) is significantly lower as compared to symmetric PEDOT:PSS based Cell 1 due to practically finite but high capacitance of $LiFePO_4$ in comparison to PEDOT:PSS.

Table 1: Comparative electrical parameters of capacitor cells from the impedance analysis

Cell	R_b or ESR (Ω cm^2)	R* (Ω cm^2)	Z' (Ω cm^2)	C_o (mF cm^{-2})	C_{sp} (F g^{-1})
1	2.96	130	-1966	8.09	26.1
2	5.38	1562	-1819	8.75	14.1

The cyclic voltammetry has been performed on the two electrode solid-state cells to investigate the electrochemical aspects. **Fig. 4** depicts the cyclic voltammograms of both cells. The CV curve of cell 1 shows symmetric redox peaks which is typical characteristic of pseudocapacitor, when CV recorded in the potential range from -0.8 to +0.8 (**Fig. 4A**). The peak nature of CV gets disappeared, when asymmetric CV pattern recorded at 10 mV s^{-1} from 0 to 2.5 V as shown in **Fig. 4B(a)**. It is also noticed that the CV patterns are observed to be deviated from the rectangular profile. The voltammetric profiles of hybrid BatCap (cell 2) show lower voltammetric currents due to resistive nature of $LiFePO_4$ electrode. In addition redox feature (i.e. oxidation and reduction peak) appears at 2.21 and 1.49 V, respectively. This can be attributed to redox reaction which is owing to the following reaction:

$$Li_{1-x}FePO_4 + x\,Li^+ + x\,e^- \Longleftrightarrow LiFePO_4 \qquad (2)$$

The sharp peak of oxidation reaction is observed while a broad hump of reduction is obtained as shown in **Fig. 4B(b)**. **Fig. 4** (**C** and **D**) depicts the CV patterns of Cell 2 at different scan rates. It is noticed that the oxidation peaks remain same while the reduction peaks are shifted to lower potential indicated by arrow (**Fig. 4D**). The reduction peaks are prominently observed in the range between 70 and 100 mV s^{-1} (**Fig. 4C**) at higher scan rates (**Fig. 4D**).

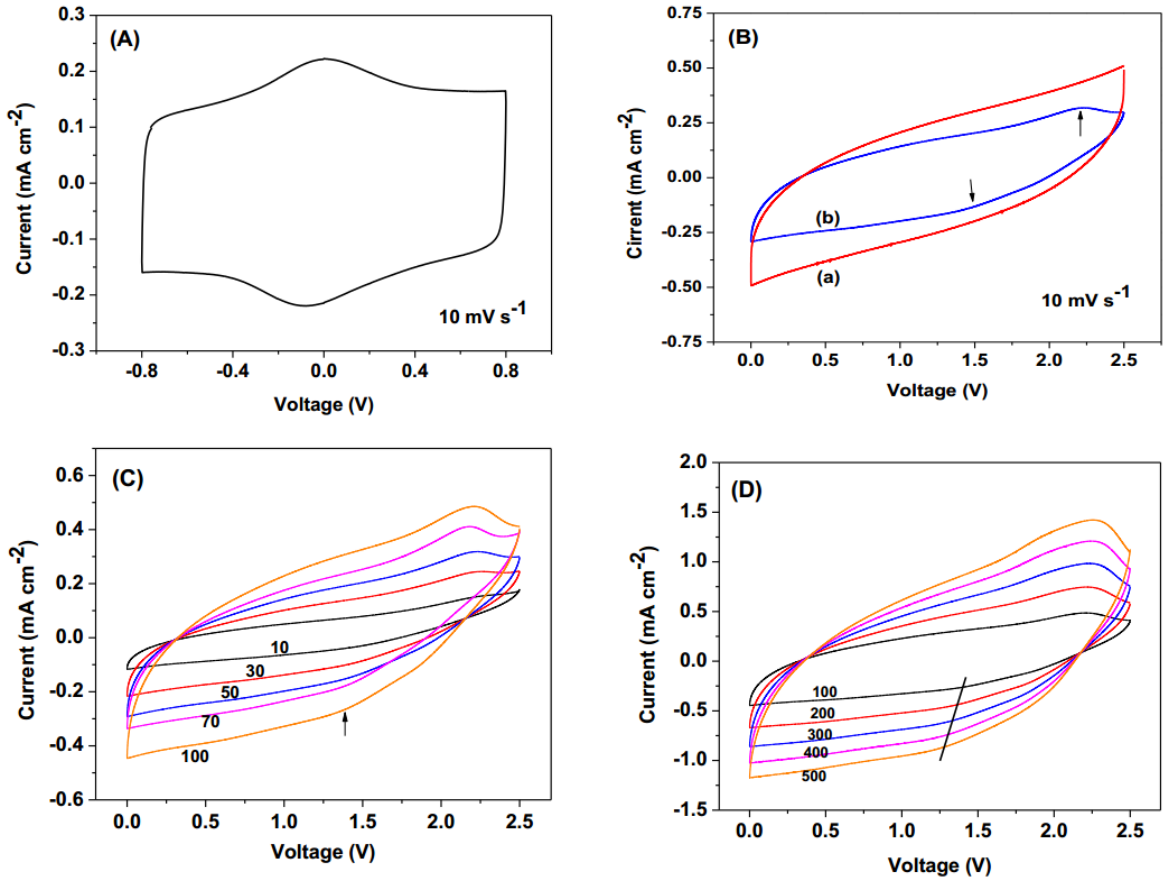

Figure 4: (A) Cyclic voltammogram of the pseudocapacitor cell 1, (B) Comparative CV curves of (a) cell 1 and (b) cell 2 at scan rat 10 mV s^{-1}, and (C and D) CVs of hybrid BatCap cell 2 at different scan rates. Scan rates (in mV s^{-1}) are marked on each voltammogram.

Almost linear charge-discharge pattern has been observed for cell 1 up to optimized voltage of 1 V showing columbic efficiency of 99%. The hybrid BatCap cell 2 shows the mixed characteristics of a capacitor (linear) and a battery (plateau region) indicating the hybrid nature of the devices with the combination of capacitive and battery-type interfaces as shown in **Fig. 5A(b)**. The hybrid cells store energy via both the fast-faradaic (pseudo-redox reaction) at capacitive PEDOT:PSS/GPE interface of all kinds of ions (Li^+, BMP^+ and $TFSI^-$) at the capacitive interface and predominantly Li^+ insertion/de-insertion at battery $LiFePO_4$/GPE interface.

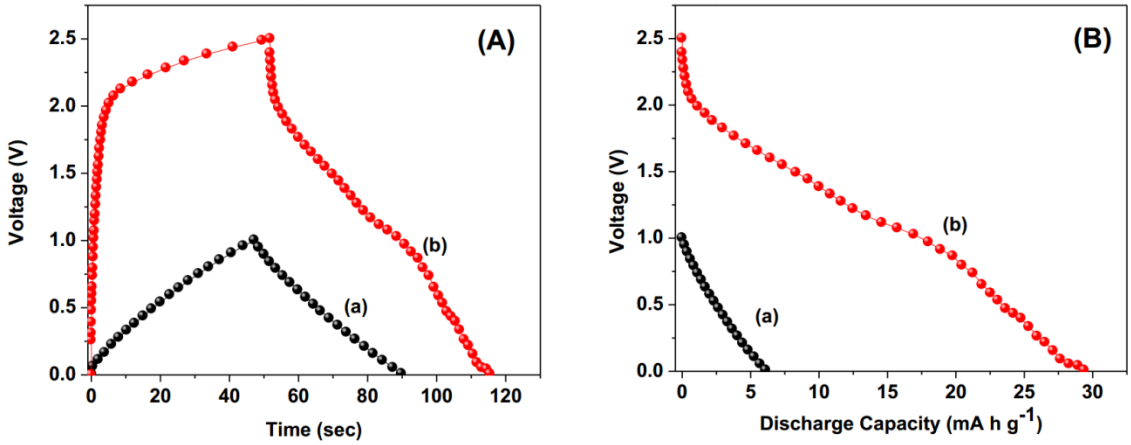

Figure 5: (A) Galvanostatic charge-discharge curves at 1 mA cm^{-2} (1 A g^{-1}), (B) Expanded representations of discharge profiles (i.e. specific capacity versus voltage profiles) of the (a) symmetric psuedocapacitor cell 1 and (b) hybrid BatCap cell 2.

Table 2: Various parameters evaluated from charge-discharge profiles at a current density of 1 A g^{-1}.

Cell	Discharge capacity (mA h g^{-1})	Energy density (Wh kg^{-1})	Power density (kW kg^{-1})
1	6.1	5.9	0.5
2	29.4	21.3	1.2

It is noticed that a plateau region for the cell 2 (with $LiFePO_4$ cathode) has been observed which improved the performance of the cell. This has been ascertained by quantitative estimation of the specific capacity listed in **Table 2**. Cell 1 with symmetric PEDOT:PSS shows the initial capacity of 6.1 mA h g^{-1} while cell 2 with $LiFePO_4$ cathode offers the approximately fifth times enhanced capacity of 29.4 mA h g^{-1}. The specific capacity of hybrid BatCap (cell 2) is found to be higher due to redox reaction involved at $LiFePO_4$ cathode in the charge storage process. The other important parameters specific energy (E) and power (P) of the cells have been evaluated by integrating the discharge curves using the expression,

$$E = \int V \times I \, dt / M \qquad (3)$$

M is the mass of electrodes including graphite powder and binder and I is constant drain current. The specific power (P) has been evaluated by using $P = E/t$, where t is the discharge time. These values of the cells have been evaluated at the constant current load of 1 mA cm^{-2} (1 A g^{-1}) and also listed in **Table 2**. About four-fold improvement in the specific energy has been observed in the hybrid cell as compared to the symmetric supercapacitor. This directly indicates the role of energetic $LiFePO_4$ cathode in the hybrid BatCap. About two times increase in the specific power has also been observed in cell 2 as compared to cell 1.

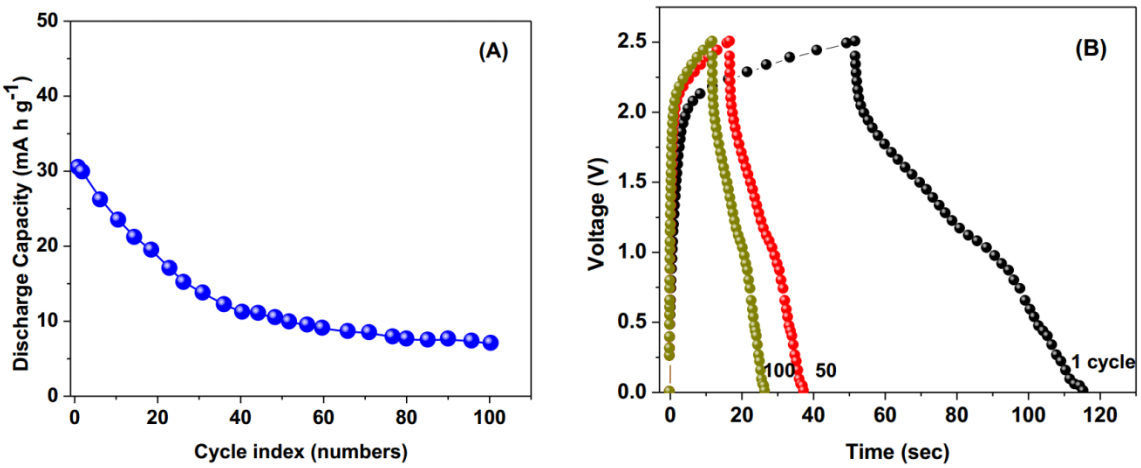

Figure 6: (A) Cyclic performance of the hybrid BatCap and (B) charge-discharge profile in 1, 50 100th cycles.

The cyclic performance is another aspect associated with hybrid BatCaps. The cyclic performance has been evaluated by galvanostatic charge-discharge tests at constant current of 1 A g^{-1} for 100 cycles as shown in **Fig. 6(A)**. The behavior of charge-discharge pattern of cell 2 after the 1st, 50th and 100th cycles are shown in **Fig. 6(B)**. After initial fading (67% in 40 cycles), the cell shows almost stable discharge capacity of 10 mA h g^{-1}. Such initial fading is observed due to the consumption of ions (Li^+, BMP^+, and $TFSI^-$) in irreversible electrochemical reactions with adsorbed surface groups like OH^- species etc., which can be further improved by using composite electrode and more wet electrolytes.

4. Conclusions

The solid-state symmetric pseudocapacitor PEDOT:PSS//PEDOT:PSS and hybrid BatCap PEDOT:PSS//$LiFePO_4$ have been fabricated using PVdF-HFP/BMPTFSI/LiTFSI gel polymer as electrolyte/separator. The $LiFePO_4$ cathode has been successfully prepared by sol-gel method and confirmed by x-ray technique. The GPE film, which offers room temperature ionic conductivity of 1.38×10^{-3} S cm^{-1} and ESW of 2.9 V, has been found to be a suitable electrolyte/separator for the supercapacitor system. The charge-discharge studies of the BatCap cell indicates its hybrid nature (PEDOT:PSS//$LiFePO_4$) as it shows a predominant plateau region. An enhanced performance of hybrid BatCap has been observed in terms of specific capacity, specific energy, specific power as compared to the pseudocapacitor PEDOT:PSS//PEDOT:PSS.

Acknowledgement

The authours acknowlege the financial support recived from University of Delhi (India) in the form of R & D grant.

References

1. Z. Chen, J.R. Dahn, J. Electrochem. Soc. 149 (2002) A1184-A1189.
2. M. Konarova, I. Taniguchi, Powder Technol. 191 (2009) 111–116.
3. S.T. Myung, S. Komaba, N. Hirosaki, H. Yashiro, N. Kumagai, Electrochim. Acta 49 (2004) 4213–4222.
4. A.A. Salah, A. Mauger, K. Zaghib, J.B. Goodenough, N. Ravet, M. Gauthier, F. Gendron, C.M. Juliena, J. Electrochem. Soc. 153 (2006) A1692-1701.
5. D. Lepage, C. Michot, G. Liang, M. Gauthier, S.B. Schougaard, Angew. Chem. Int. Ed. Engl. 50 (2011) 6884-6887.
6. T. Brousse, D. Belanger, D. Guay, Asymmtric and Hybrid Devices in aquous electrolyte, in: F. Beguin, E Frackowiak (Eds.), Supercapacitor: Materials, System, and Applications, Wiley-VCH Verlag GmbH & Co. KGaA, Germany, 2013.
7. K. Naoi, P. Simon, The Electrochemical Society Interface, Spring 17 (2008) 34-37.
8. H.S. Choi, J.H. Im, T. Kim, J.H. Park, C.R. Park, J. Mater. Chem. 22 (2012) 16986-19993.
9. D. Cericola, R. Kötz, Electrochim. Acta. 72 (2012) 1–17.
10. G.A. Snook, P. Kao, A.S. Best, J. Power Sources 196 (2011) 1−12.
11. J.B. Goodenough, K.S. Park, J Am ChemSoc 135 (2013) 1167–1176.
12. L.X. Yuan, Z.H. Wang, W.X. Zhang, X.L. Hu, J.T. Chen, Y.H. Huang, J.B. Goodenough, Energy Environ. Sci. 4 (2011) 269-284.

13. F. Beguin, E. Frackowiak (Eds.), Supercapacitor: Materials, System, and Applications, Wiley-VCH Verlag GmbH & Co. KGaA, Germany, 2013.
14. R.C. Agrawal, G.P. Pandey, J. Phys D: Appl. Phys. 41 (2008) 223001(18 pp).
15. A.M. Stephan, K.S. Nahm, Polymer 47 (2006) 5952-5964.
16. H. Ohno, Electochemical sspects of ionic liquids, New Jersey: John Wiley & Sons, Inc., Hoboken, 2005.
17. M.K. Singh, S.A. Hashmi, Ionics 23(10) (2017) 2931–2942.
18. M.K. Singh, Y. Kumar, S.A. Hashmi, Nanotechnology 24 (2013) 465704 (10 pp).
19. M.K. Singh, S.A. Hashmi, AIP Conf. Proc. 1665 (2015) 060011 (3 pp).
20. Y. Bai , Y. Yin Y, J. Yang, C. Qing, W. Zhang, J. Raman Spectroscopy 42 (2011) 831–838.
21. K.J. Rouquerol, F. Rouquerol, Adsorption by powders and porous solids: principles, methodology and applications, Academic Press, London, 1998.
22. S.A. Hong, S.J. Kim, J. Kim, B.G. Lee, K.Y. Chung, Y.W. Lee, Chem. Eng. J. 198 (2012) 318-326.
23. B.E. Conway, W.G. Pell, J. Solid State Electrochem. 7 (2003) 637-644.
24. W.G. Pell, B.E. Conway, J. Power Sources 136 (2004) 334-345.
25. H. Zhang, Y. Chen, C. Zheng, D. Zhang, C. He, Ionics 21 (2015) 1813-1818.

© 2017 by the authors. Published by EMS (www.electroactmater.com). This article is an open access article distributed under the terms and conditions of the Creative Commons Attribution license (http://creativecommons.org/licenses/by/4.0/).